arXiv:1412.7916v1 [astro-ph.GA] 26 Dec 2014

# Parallaxes of Star Forming Regions in the Outer Spiral Arm of the Milky Way

K. Hachisuka[1,2,3], Y. K. Choi[4,6], M. J. Reid[5], A. Brunthaler[6], K. M. Menten[6], A. Sanna[6], T. M. Dame[5]

## ABSTRACT

We report parallaxes and proper motions of three water maser sources in high-mass star-forming regions in the Outer Spiral Arm of the Milky Way. The observations were conducted with the Very Long Baseline Array as part of Bar and Spiral Structure Legacy Survey and double the number of such measurements in the literature. The Outer Arm has a pitch angle of $14\overset{\circ}{.}9 \pm 2\overset{\circ}{.}7$ and a Galactocentric distance of $14.1 \pm 0.6$ kpc toward the Galactic anticenter. The average motion of these sources toward the Galactic center is $10.7 \pm 2.1$ km s$^{-1}$ and we see no sign of a significant fall in the rotation curve out to 15 kpc from the Galactic center. The three-dimensional locations of these star-forming regions are consistent with a Galactic warp of several hundred parsecs from the plane.

*Subject headings:* astrometry - Galaxy: kinematics and dynamics - Galaxy: structure - masers - stars: distances

## 1. Introduction

Looking outward from the Sun in the direction of the Galactic anticenter, one's sight line passes through the Local, Perseus and Outer spiral arms of the Milky Way (e.g. Xu

[1]Research Institute for Time Studies, Yamaguchi University, Yoshida 1677-1, Yamaguchi, Yamaguchi, 753-8511, Japan

[2]Shanghai Astronomical Observatory, Chinese Academy of Science, 80 Nandan Road, Shanghai, 200030, China

[3]Center for Astronomy, Ibaraki University, 2-1-1 Bunkyo, Mito, Ibaraki 210-8512, Japan

[4]Korea Astronomy and Space Institute, Daedeokdae-ro 776, Yuseong-gu, Daejeon, 305-348, Korea

[5]Harvard-Smithsonian Center for Astrophysics, 60 Garden Street, Cambridge, MA 02138, USA

[6]Max-Planck-Institut für Radioastronomie, Auf dem Hügel 69, D-53121, Bonn, Germany

et al. 2013; Choi et al. 2014; Dame et al. 2001; Vallée 2005; Churchwell et al. 2009; Reid et al. 2014).The Outer Arm may originate near the Galactic bar (McClure-Griffiths et al. 2004; Nakanishi & Sofue 2006; Levine et al. 2006; Dame & Thaddeus 2011) and wind its way outward through more than 360 deg of Galactocentric azimuth, until reaching and then passing the anticenter direction. While, for example, there is prolific star formation in the Perseus arm, there is relatively little activity in the Outer Arm in the second and third quadrants. This makes it challenging to accurately trace its structure and determine kinematic properties.

Trigonometric parallax distances, $D_\pi$, have been measured for only three 22 GHz water maser sources in the Outer Arm: $D_\pi = 9.25 \pm 0.43$ kpc for G075.30+01.32 (Sanna et al. 2012), $D_\pi = 5.99 \pm 0.22$ kpc for WB 89–437 (G135.27+02.79) (Hachisuka et al. 2009), and $D_\pi = 5.28 \pm 0.23$ kpc (Honma et al. 2007) or $D_\pi = 4.05 \pm 0.65$ kpc (Asaki et al. 2014) for S 269 (G196.45–01.67). While clearly more astrometric data are desirable in order to better understand the properties of the Outer Arm, few maser sources have been discovered, owing to the low star formation rate and general weakness of these masers (e.g. Wouterloot et al. 1993; Szymczak & Kus 2000).

Astrometry with Very Long Baseline Interferometry (VLBI) can yield trigonometric parallaxes with accuracies better than $\pm 10$ $\mu$as and is an excellent tool to study Galactic structure and dynamics (e.g. Reid et al. 2009b; Honma et al 2012; Reid et al. 2014). In this paper, we report parallaxes and proper motions of three water masers associated with high-mass star-forming regions (HMSFRs): G097.53+03.18, G168.06+00.82 and G182.67−03.26. These measurements are part of the Bar and Spiral Structure Legacy (BeSSeL) Survey and double the number of sources with accurate parallaxes in the Outer Arm.

## 2. Observations

We used the National Radio Astronomy Observatory's (NRAO) [1] Very Long Baseline Array (VLBA) to observe 22 GHz water maser sources under programs BR145G, H, and V. We observed with four adjacent 8 MHz bands in right and left circular polarization, with the second band centered on the water maser. The continuum and line data were correlated with the VLBA DiFX [2], producing 16 and 256 spectral channels per band, respectively. Ad-

[1]The National Radio Astronomy Observatory is a facility of the National Science Foundation operated under cooperative agreement by Associated Universities, Inc.

[2]DiFX, a software Correlator for VLBI, is developed as part of the Australian Major National Research Facilities Programme by the Swinburne University of Technology and operated under license.

ditionally, we placed four "geodetic blocks" throughout each seven hour track, as described in Reid et al. (2009a), in order to measure and remove residual tropospheric delays relative to the correlator model. The parallax observations involved rapid switching between compact extragalactic continuum sources and water maser sources. For each maser source, we observed at six epochs spanning one year (see Tables 1 and 2 for details), with a sequence designed to yield good parallax results for a maser spot that might last only seven months. Data reduction was performed using the NRAO Astronomical Image Processing System, as described in Reid et al. (2009a).

The water masers were detected at all epochs, and generally we chose a strong, compact maser spot to use as the interferometer phase reference. The second continuum source associated with G182.68−03.26, while detected at the first epoch, was not useful for parallax results owing to its large angular separation (3°) from the maser.

Table 1: Source Information.

| Source | Type | R.A. (J2000) (h m s) | Decl. (J2000) (° ' ") | $\theta_{sep}$ (°) | P.A. (°) | Brightness (mJy beam$^{-1}$) | N |
|---|---|---|---|---|---|---|---|
| G097.53+03.18 | M | 21:32:12.4343 | +55:53:49.689 | – | – | – | 11 |
| J2127+5528 | C | 21:27:32.27527 | +55:28:33.9771 | 0.78 | -122 | 11 | |
| J2139+5540 | C | 21:39:32.61754 | +55:40:31.7711 | 1.05 | 101 | 16 | |
| J2123+5500 | C | 21:23:05.31350 | +55:00:27.3250 | 1.57 | -124 | 94 | |
| J2117+5431 | C | 21:17:56.48440 | +54:31:32.5030 | 2.45 | -123 | 92 | |
| G168.06+00.82 | M | 05:17:13.7436 | +39:22:19.915 | – | – | – | 4 |
| J0523+3926 | C | 05:23:51.2364 | +39:26:57.736 | 1.28 | 86 | 17 | |
| J0509+3951 | C | 05:09:48.8173 | +39:51:54.618 | 1.51 | -70 | 69 | |
| J0512+4041 | C | 05:12:52.5428 | +40:41:43.620 | 1.56 | -32 | 224 | |
| G182.68–03.26 | M | 05:39:28.4248 | +24:56:31.946 | – | – | – | 4 |
| J0540+2507 | C | 05:40:14.3428 | +25:07:55.349 | 0.26 | 42 | 12 | |
| J0550+2326 | C | 05:50:47.3909 | +23:26:48.177 | 2.98 | 120 | 33 | |

**Notes.** Type: M for maser source; C for continuum source; $\theta_{sep}$ and P.A. are angular separation and position angle east of north from each maser source. N is number of maser spots for astrometric fitting.

Table 2: Observation Epochs

| Source | Epoch | | | | | |
|---|---|---|---|---|---|---|
| | 1st | 2nd | 3rd | 4th | 5th | 6th |
| G097.53+03.18 | 2010/Dec/10 | 2011/Feb/21 | 2011/Apr/30 | 2011/May/29 | 2011/Jul/17 | 2011/Nov/17 |
| G168.06+00.82 | 2010/Apr/16 | 2010/Jun/17 | 2010/Aug/15 | 2010/Sep/24 | 2010/Nov/15 | 2011/Mar/7 |
| G182.68−03.26 | 2010/Apr/23 | 2010/Jun/20 | 2010/Aug/23 | 2010/Sep/25 | 2010/Nov/16 | 2011/Mar/21 |

Table 3: Parallax and Proper Motions

| Name | $\pi$ (mas) | $\mu_{\rm X}$ ($\mu$as) | $\mu_{\rm y}$ ($\mu$as) | $V_{\rm LSR}$ (km s$^{-1}$) |
|---|---|---|---|---|
| G097.53+03.18 | 0.133± 0.017 | –2.94± 0.06 | –2.48± 0.14 | –75± 3 |
| G168.06+00.82 | 0.201± 0.024 | 0.58± 0.31 | –0.78± 0.31 | –28± 5 |
| G182.67-03.26 | 0.157± 0.042 | 0.44± 0.34 | –0.45± 0.35 | –8 ±10 |

**Notes.** Columns 1 through 5 give the source name, annual parallax ($\pi$), absolute proper motion in the eastward ($\mu_{\rm X}$) and northward ($\mu_{\rm y}$) directions, and the mean Local Standard of Rest velocity ($V_{\rm LSR}$). The uncertainty assigned to $V_{\rm LSR}$ is the difference between mean velocity of masers and of thermal CO emission from the parent molecular cloud, except for G182.67-03.26 where there is no information for thermal molecular lines and we adopt an uncertainty of 10 km s$^{-1}$ (Wouterloot et al. 1995). Other characteristics of these sources can be found Section 3.1, 3.2 and 3.3.

## 3. Astrometric Results

Source positions were estimated by fitting an elliptical Gaussian brightness distribution to the interferometric images. These fits produced formal position uncertainties, which do not include systematic sources of error, typically dominated by uncompensated atmospheric delays. Therefore, during the fitting process, we included"error floors" to account for these systematic uncertainties. The error floors were added in quadrature to the formal position uncertainties and adjusted until we achieved $\chi^2_\nu$ per degree of freedom values of near unity in each coordinate. The parallax and absolute proper motion results are shown in Table 3. When we report an annual parallax by combining two or more maser spots, we multiplied the formal fitting error by $\sqrt{N}$, where $N$ is the number of maser spots, conservatively allowing for the possibility of 100% correlated position uncertainties among the spots. Throughout this paper we adopt customary definitions for a maser spot (the emission in one spectral channel) and maser feature (typically several channels that comprise a Gaussian line shape). On the one hand, only the most compact maser spots, detected at all epochs, were used to fit the parallax curve. On the other hand, in order to estimate the Galactic proper motion of

the star-forming region, we took into account the internal motions of as many maser spots as possible. Their average motion has been taken as representative of the motion of the central star and was used to correct the proper motion value inferred with the parallax fitting (Table 3).

Water masers are typically associated with outflowing motions from young stellar objects tracing velocities on the order of tens of km $s^{-1}$. For the line-of-sight velocity component, we rely on emission from thermal lines of CO and other molecules, which sample larger portions of the molecular cloud, to provide a more robust estimate of the average motion of the central star.

### 3.1. G097.53+03.18

This region, also known as S 128, consists of a diffuse and compact H II region. The 22 GHz water masers are located near the northern compact H II region (S 128N; Haschick & Ho ). There are also two water maser spots separated by about 9″ from S 128N, (Haschick & Ho 1985), but these were not imaged owing to fringe-rate smearing. The LSR velocity for CO emission is −74 km $s^{-1}$ (Haschick & Ho 1985) and for CS emissionis −70 km $s^{-1}$ (Plume et al. 1997). The water masers have LSR velocitiesfrom −69 to −83 km $s^{-1}$, with the peak brightness at −77 km $s^{-1}$.

We choose 11 maser spots from seven different maser features for the parallax and proper motion fitting. The results for the maser spots and background continuum sources are listed in Tables 5. The parallax and proper motion data for the maser spot at $V_{\rm LSR}$= −77.0 km $s^{-1}$ are shown in Figure 1. The distribution of maser features is complex we fitted a uniformly expanding source model (Sato et al. 2010), giving the results shown in Figure 2. On average, maser features are expanding slowly ($2.2 \pm 5.3$ km $s^{-1}$) and the average proper motion of the central exciting star(s) is $0.33 \pm 0.15$ mas $yr^{-1}$ eastward and $0.01 \pm 0.15$ mas $yr^{-1}$ northward.

### 3.2. G168.06+00.82

This source is also known as Mol 8 (Brand et al. 2001). The 22 GHz water masers are located toward the peak emission from thermal molecular lines (Brand et al. 2001) and millimeter-wavelength dust continuum (Molinari et al. 2000). The LSR velocity peaks for $HCO^+$, $^{13}CO$ and CS are all near −25 km $s^{-1}$. The radial velocity range of the water masers is small, from −25 to −31 km $s^{-1}$, reasonably close to the thermal line peaks.

Several maser features were detected at all epochs and we choose four maser spots from

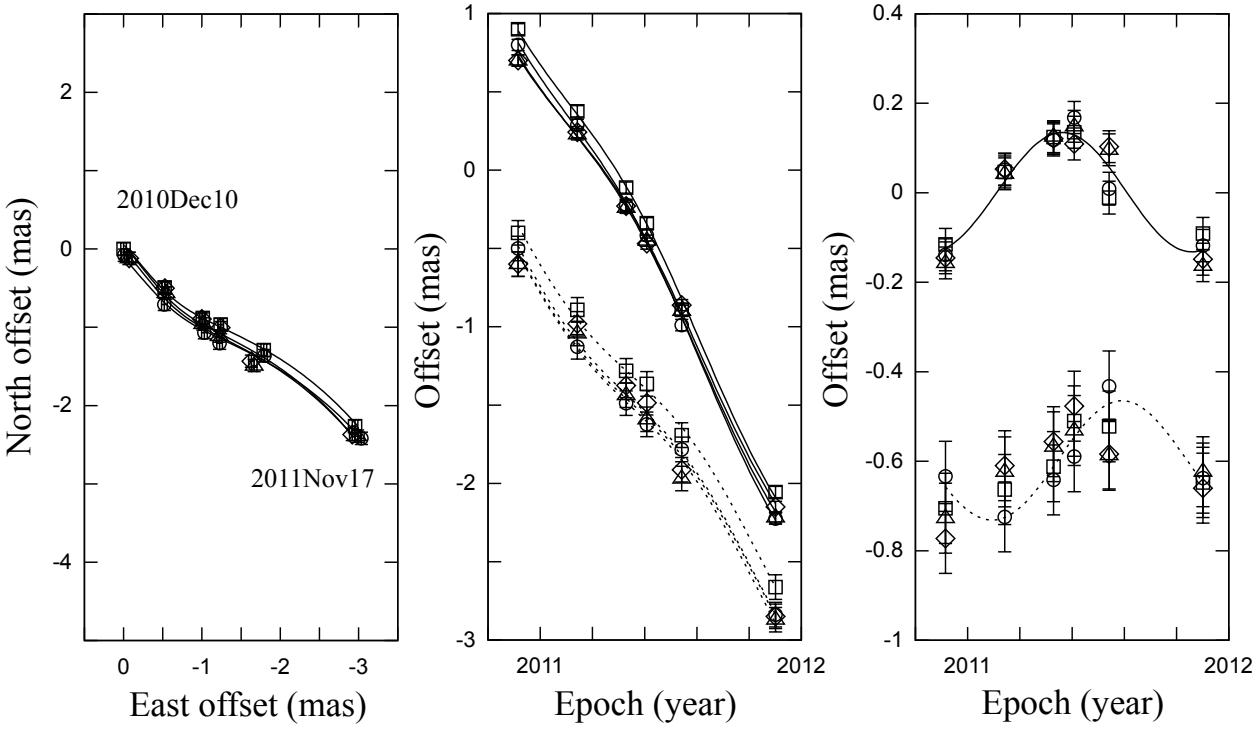


Fig. 1.— Parallax and proper motion data for the maser spot at $V_{\rm LSR}= -77.0$ km s$^{-1}$ toward G097.53+03.18 relative to the background sources J2127+5528 (squares), J2139+5540 (circles), J2123+5500 (triangles) and J2117+5431 (diamonds). *Left panel:* position offsets on the sky. *Center panel:* offsets of maser spots eastward (*solid line*) and northward (*dashed line*) vs. time. *Right panel:* same as the center panel, but with the proper motion removed.

one feature and one maser spot from other feature for astrometric fitting (see Table 6). Other maser spots in other features were not used for the astrometic fitting because they displayed complex, time varying blended structures. The combined annual parallax and average absolute proper motion are shown in Table 3. The parallax and proper motion fit for the maser spot at an LSR velocity of $-28.74$ km s$^{-1}$ is shown in Figure 3.

Honma et al. (2011) measured the parallax and proper motion of the water masers in this source (also known as IRAS 05137+3919). Their parallax is based on two maser features (one feature detected in five spectral channels), neither detected over a time span longer than $\approx 0.6$ yr. Honma et al. favor a weighted parallax of $0.086 \pm 0.027$ mas. If one adopts their solution with equal weights for the two features and allows for the parallax estimates of these features being correlated (as expected for atmospheric mis-modeling being the dominant source of systematic uncertainty), then their parallax result would be $0.103 \pm 0.030$ mas. There is some tension with our result of $0.201 \pm 0.024$ mas, as the difference between the

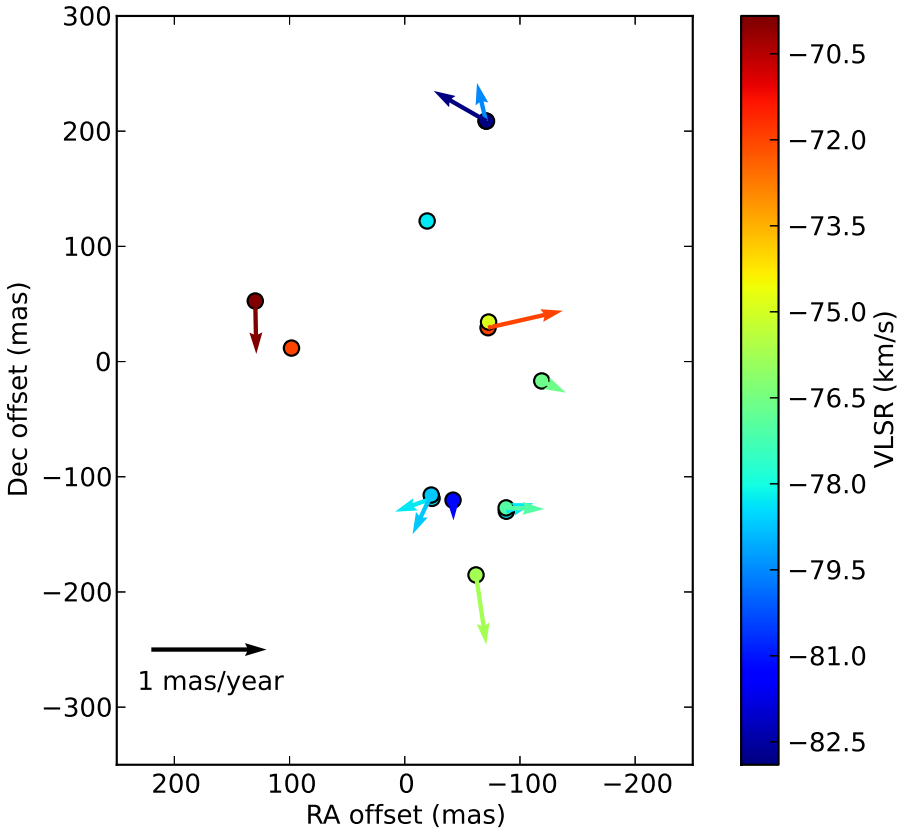


Fig. 2.— Proper motions of water masers toward G097.53+03.18. Vectors indicate motions about the estimated center of expansion near (0,0) mas. Spots without vectors indicate that the maser was detected only at one or two epochs.

two measurements would be $0.098 \pm 0.039$ mas.

Even though this source has only a small number of maser features, we did fit an expanding flow in order to estimate the central star's motion. However, we conservatively assign an large uncertainty of $\pm 7$ km s$^{-1}$ ( $\sim$0.3 mas yr$^{-1}$ at 5.0 kpc) for the components of proper motion of the central star. The internal motions of maser features with the central star's estimated motion removed are shown in Figure 4.

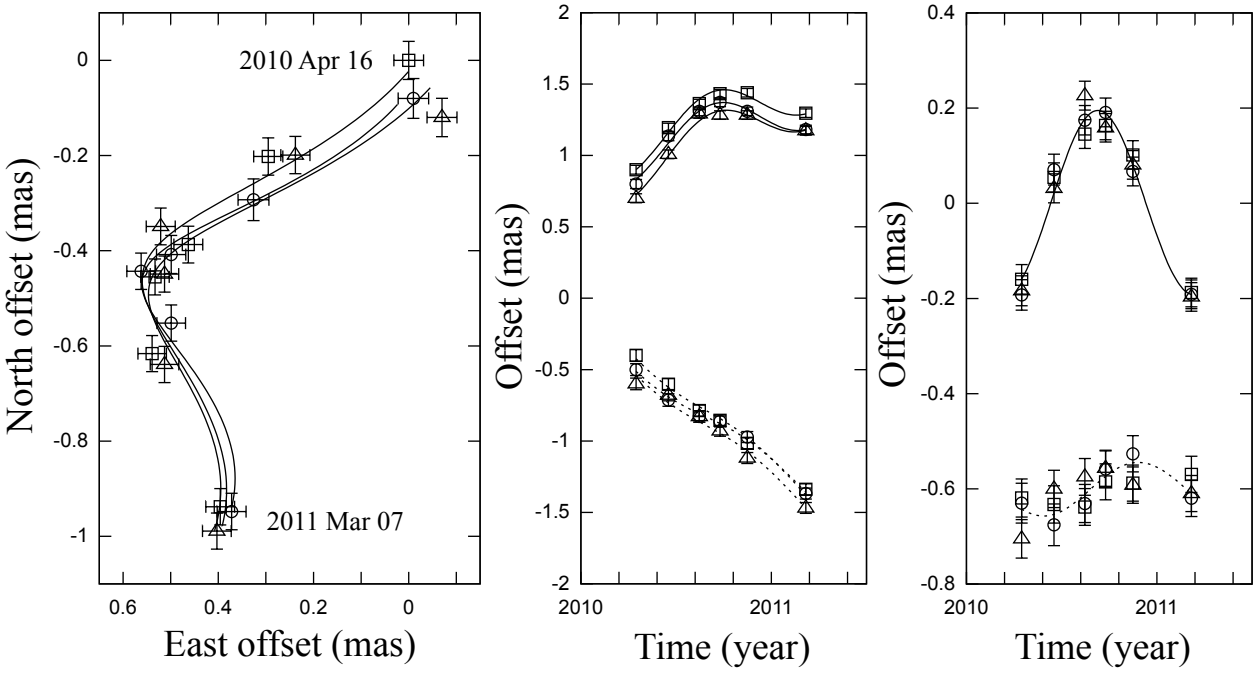


Fig. 3.— Annual parallax and proper motion of the maser spot at $V_{\rm LSR}$=−28.74 km s$^{-1}$ toward G168.06+00.82 relative to background source, J0512+4041 (squares), J0523+3926 (circles) and J0509+3951 (triangles). See Figure 1 caption for details.

### 3.3. G182.67–03.26

We are unaware of measurements of thermal emission from molecular lines in the literature for this source. The radial velocity range of the 22 GHz water masers is very small, −5 to −9 km s$^{-1}$. Four maser spots at three different positions were detected at all epochs spanning one year, and we used these spots for the astrometric fitting (see Table 7). The parallax and proper motion of the maser spot at $V_{\rm LSR}$= −5.79 km s$^{-1}$ is shown in Figure 5. The combined parallax for maser spots is $0.157 \pm 0.042$ mas, corresponding to a distance of 6.4 kpc.

Estimating the absolute motion of the central exciting star is difficult in this source, since only three maser features were detected. The mean proper motion for the three maser features that could be traced for two or more epochs was $0.35 \pm 0.23$ mas yr$^{-1}$ eastward and $-0.14 \pm 0.47$ mas yr$^{-1}$ northward, or $11 \pm 7$ km s$^{-1}$ and $4 \pm 14$ km s$^{-1}$ at the distance of 6.4 kpc. Owing to the minimal number of maser spots with measured motions, we conservatively add ( 10 km s$^{-1}$)/( 6.7 kpc ) =0.33 mas yr$^{-1}$ in quadrature with the measurement uncertainty when transferring the maser motion to that of the central star.

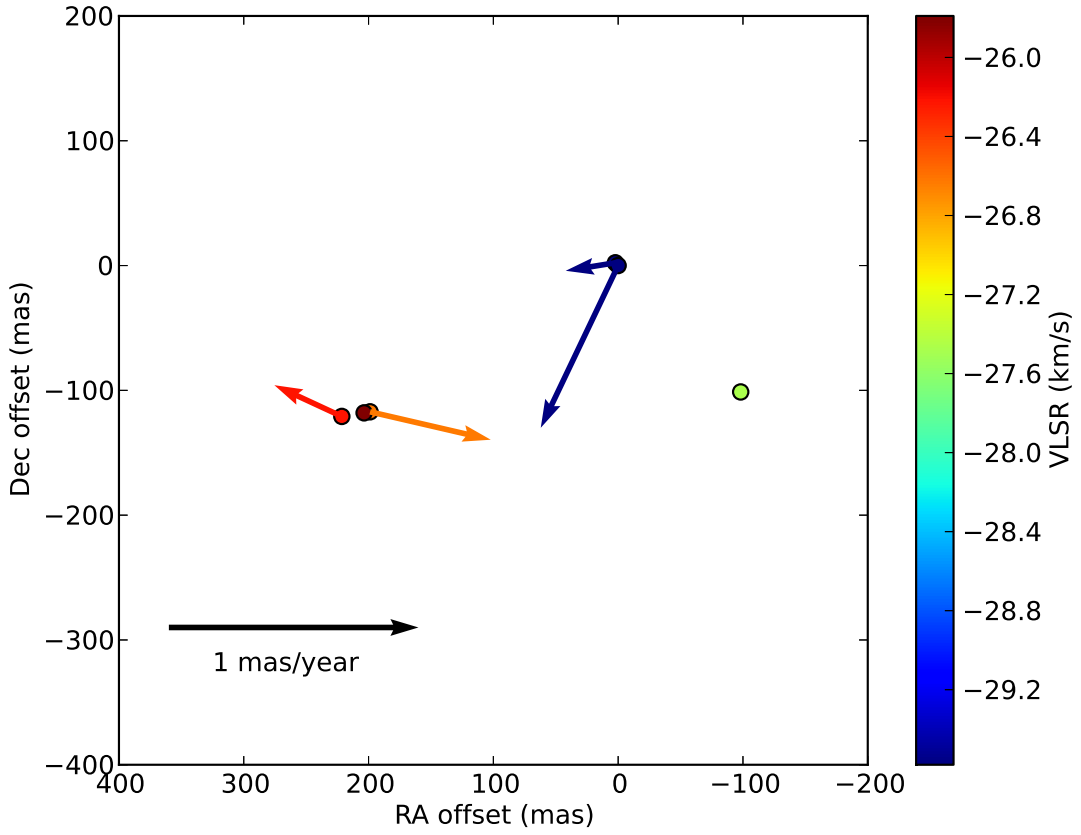


Fig. 4.— Proper motions of water masers toward G168.06+00.82. Vectors indicate motions about the estimated center of expansion near (0,0) mas. Spots without vectors indicate that the maser was detected only one or two epochs.

## 4. Discussion

There are now VLBI astrometric observations toward six 22 GHz water maser sources in the outer spiral arm of the Milky Way (see Table 4). The locations of these HMSFRs in the Galaxy and their peculiar motions relative to a Galactic rotation model are given in Table 4. The peculiar motions assumed a flat rotation curve with $\Theta = 239 \pm 7$ km s$^{-1}$ and the distance to the Galactic center of $R_0 = 8.3 \pm 0.2$ kpc (Brunthaler et al. 2011), and the Solar motion of $(U_s, V_s, W_s) = (11.10, 12.24, 7.25)$ km s$^{-1}$(Schönrich et al. 2010).

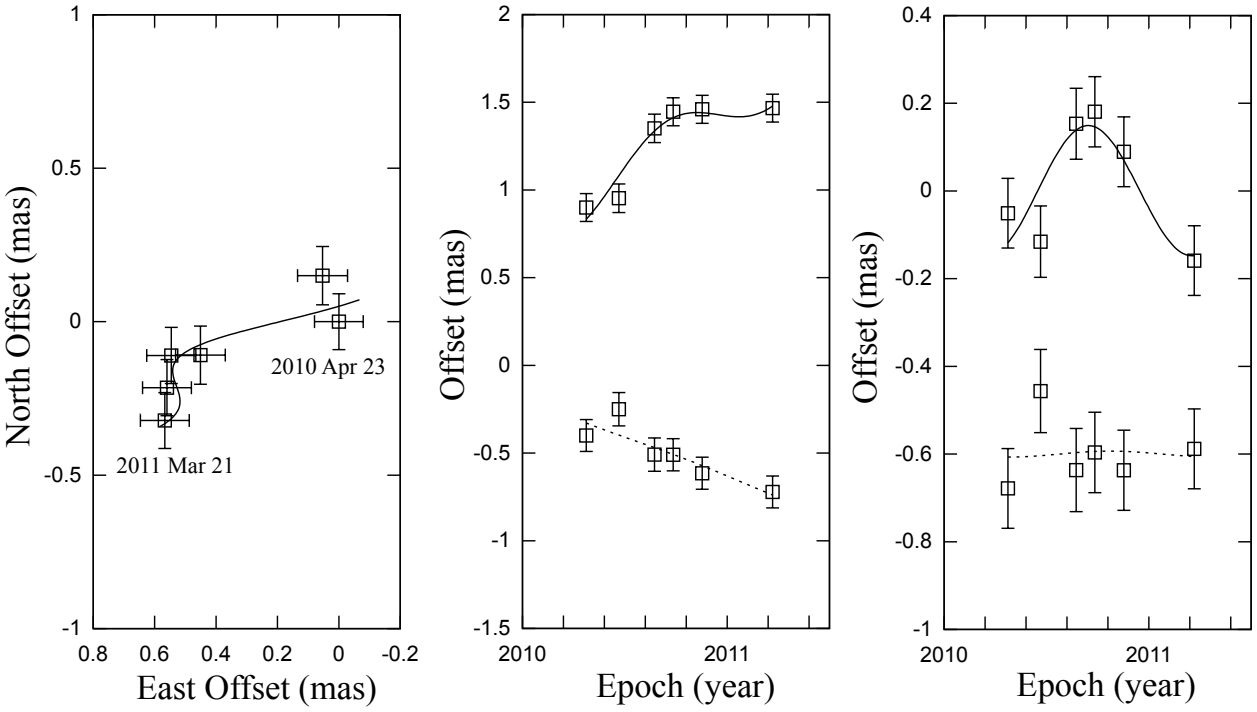


Fig. 5.— Annual parallax and proper motion of the maser spot at $V_{\rm LSR}$=−7.89 km s$^{-1}$ toward G182.67–03.26 relative to background source J0540+2507. See Figure 1 for details.

### 4.1. Structure of the Outer arm

The Outer Arm as it passes through the second and third Galactic quadrants should be close to the outer "edge" of the spiral structure as traced by stars, and its location may mark the outer range of active star formation in the Milky Way. With six sources in the Outer Arm, spanning a large range of Galactocentric azimuth, $\beta$ (the angle between the Sun and a source as viewed from the Galactic center and increasing with Galactic longitude), we estimate the pitch angle by fitting a section of a log-periodic spiral pattern to $\ln(R/{\rm kpc})$ versus $\beta$, as described in Reid et al (2014). The data are plotted in Figure 6 and the pitch angle is estimated to be $14\overset{\circ}{.}9 \pm 2\overset{\circ}{.}7$. This estimate is consistent within $1\sigma$ with the value reported in Reid et al (2014), which included the contribution of the star forming region G196.45-01.67 as well. Also, our estimate agrees within $2\sigma$-$3\sigma$ with the range of pitch angles reported by Hou & Han (2014), who made use of a compilation of different star formation tracers

The Galactocentric distance of Outer Arm at $\beta = 0$ (toward the Galactic anticenter) is $14.1 \pm 0.6$ kpc. This is consistent with the size of stellar disk estimated from red-clump giant stars of $13.9 \pm 0.5$ kpc by Minniti et al. (2011), provided the Outer Arm dies off before

Table 4: Outer Arm Sources.

| Name | IRAS | WB89 | Other Name | $R_{GC}$ (kpc) | z (kpc) | $U_s$ (km $s^{-1}$) | $V_s$ (km $s^{-1}$) | $W_s$ (km $s^{-1}$) | Ref. |
|---|---|---|---|---|---|---|---|---|---|
| G075.29+01.32 | 20144+3726 | | | 10.75±0.50 | 0.22±0.01 | 12.0± 6.0 | 0.4±9.4 | -17.9± 6.0 | 1 |
| G097.53+03.18 | 21306+5540 | 91 | S128N | 11.90±1.52 | 0.42±0.05 | 10.8±3.6 | 1.1±14.4 | 8.9± 4.1 | 3 |
| G135.27+02.79 | 02395+6244 | 437 | | 13.24±0.87 | 0.29±0.02 | 14.8±5.3 | 2.5± 8.4 | 0.9±9.9 | 2 |
| G168.06+00.82 | 05137+3919 | 621 | | 13.21±1.58 | 0.07±0.01 | 9.8± 5.3 | -11.3± 7.9 | 4.8± 7.5 | 3 |
| G182.67–03.26 | 05363+2454 | | | 14.66±3.92 | -0.36±0.10 | 13.1±10.0 | –5.7±12.3 | 11.1±11.0 | 3 |

References:(1) Sanna et al. 2012, (2) Hachisuka et al. 2009 and (3) this paper. $(U_s, V_s, W_s)$ are the peculiar motion components toward the Galactic center, in the direction of Galactic rotation, and toward the north Galactic pole.

reaching much greater distance.

Because the Outer Arm from the second through the fourth Galactic quadrants is at a great distance from the Galactic center, the arm is subject to possible warping through interactions with other galaxies in the Local Group (e.g., Purcell et al. 2011). Warping is clearly seen for HI gas beyond the stellar disk (e.g., Levine et al. 2006). The offsets of the star-forming regions with parallax distances (spanning $75^\circ < l < 183^\circ$) perpendicular to the Galactic plane show clear signs of warping (see Table 4 and Figure 7). Urquhart et al (2014) suggest that the mean amplitude of warping for red MSX sources at a Galactocentric distance of 11.5 kpc is about 160 pc from the Galactic plane ($b = 0^\circ$), and our data show a warping reaching 400 pc at 13 kpc. This tendency is consistent with the warping of the HI disk of the Milky Way beyond 13 kpc noted by Levine et al. (2006), Kalberla et al. (2007), and Kalberla & Kerp (2009).

The annual parallax of 0.189±0.008 mas for water maser source G196.45 − 01.67 (IRAS 06117+1350 or S269) was measured by VLBI Exploration of Radio Astrometry (VERA) using one maser spot; this large distance suggested that the maser source was a part of the Outer Arm (Honma et al. 2007). Recently, Asaki et al (2014) re-analyzed the VERA data for this source using a more compact maser spot, and obtained a parallax of 0.247±0.034 mas. The revised VERA parallax distances suggests that G196.45 − 01.67 is closer to the Sun than we find by spiral arm fitting of five Outer Arm sources. Therefore, G196.45 − 01.67 might be an interam source between Perseus and Outer Arms. Indeed, two other maser sources toward the general anticenter direction found by the BeSSeL Survey (Reid et al. 2014) also seem to lie between the Perseus and Outer Arms (Figure 7). Possibly, the Outer Arm splits into two branches in this region; more astrometric results are needed to clarify this issue.

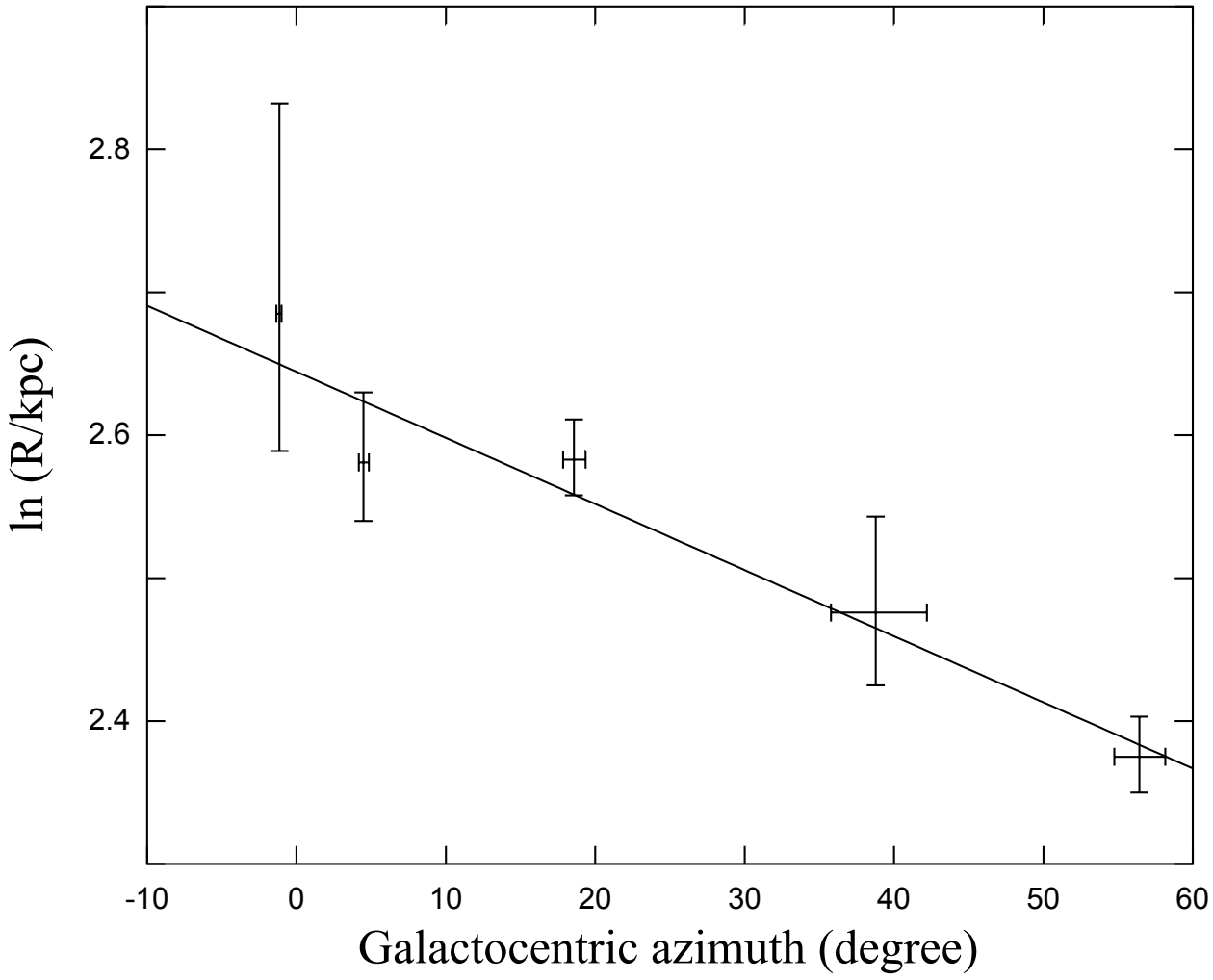


Fig. 6.— Galactocentric distance vs. azimuth. The line is the result of log-periodic spiral fitting.

### 4.2. Velocity Field in the Outer Arm

The Galactic rotation speed in the outer Galaxy is an important parameter for estimating the distribution of mass among the Galactic disk, bulge, and halo. Assuming the Galactic and Solar motion parameters given above, we find small peculiar motions in the direction of Galactic rotation ($V_s$ in Table 4) for these sources. The weighted average for $\overline{V_s}$ values is $-3.3 \pm 4.4$ km s$^{-1}$. This suggests that the Galactic rotation speed remains reasonably constant to Galactocentric distances of at least 15 kpc, supporting the existence of a dark matter halo. Although the component of peculiar motions toward the north Galactic pole ($W_s$ in Table 4) display some scatter, the weighted average ($\overline{W_s}$) of these values is $1.8 \pm 2.9$ km s$^{-1}$, which suggests that the maser sources on average are moving almost entirely in the

Galactic plane.

It is interesting to note that all five maser sources clearly identified with the Outer Arm have peculiar motion components toward the Galactic center (i.e., positive $U_s$ values in Table 4), suggesting that the sources in the Outer Arm are not in simple circular Galactic orbits. The weighted average ($\overline{U_s}$) is $11.7 \pm 2.3$ km s$^{-1}$.

### 4.3. Other Maser Sources in the Outer Srm

In order to better understand the structure and dynamics of outer Galaxy will require more astrometric data. Surveys for 6.7 GHz methanol maser sources beyond the Perseus Arm have been performed, but only a few sources have been found (Pestalozzi et al. 2005, Xu et al. 2008). Of these sources, two (G097.53 + 03.18 and G168.06 + 00.82) belong to star forming regions with 22 GHz water masers reported in this paper, and a third (G196.45 − 01.67) displays both methanol and water masers (Menten 1991; Rygl et al. 2010) and an astrometric result has been reported (Honma et al. 2007; Asaki et al 2014).

Although extensive surveys for 22 GHz water masers have been performed, only a few tens of sources have been found with Galactocentric distances that might be beyond the Perseus arm ($\gtrsim 10$ kpc; Woulterloot et al. 1993, 1988). Unfortunately, most outer Galaxy water masers are weak and upcoming parallax observations for sources in the Outer Arm will require greater sensitivity. This can be provided by the VLBA with its recent bandwidth upgrade, which allows the use of weaker background continuum sources as phase calibrators.

## 5. Summary

We have performed VLBA parallax and proper motion observations of three water maser sources associated with regions of high-mass star formation in the Outer Arm of the Milky Way. These observations are part of the BeSSeL Survey, an NRAO Key Science Project. Combining our results with published results, we find that the Galactocentric distance of the Outer Arm is $14.1 \pm 0.6$ kpc in the direction of the anticenter, which is consistent with estimates of the outer edge of the stellar disk. The pitch angle of the Outer Arm in the second and third Galactic quadrants is $14\overset{\circ}{.}9 \pm 2\overset{\circ}{.}7$. Our findings, though based on a limited number of sources, indicate a tendency for peculiar motions toward the Galactic center, as might be expected for gas entering a trailing spiral arm and being shock and then forming stars. In order to better determine the structure of the Outer Arm, further astrometric observation of weak water maser sources are needed.

This work is partly supported by China Ministry of Science and Technology under State Key Development Program for Basic Research (2012CB821800), the National Natural Science Foundation of China (grants 10625314, 11121062). The authors acknowledge the financial support by the European Research Council for the ERC Advanced Grant GLOSTAR under contract no. 247078.

*Facilities:* VLBA

## REFERENCES

Asaki, Y., Imai, H., Sobolev, A. M., & Parfenov, S. Y. 2014, ApJ, 787, 54

Brand, J., Cesaroni, R., Palla, F., & Molinari, S. 2001, A&A, 370, 230

Brunthaler, A., Reid, M. J., Menten, K. M., et al. 2011, Astronomische Nachrichten, 332, 461

Choi, Y. K., Hachisuka, K., Reid, M. J., et al. 2014, ApJ, 790, 99

Churchwell, E., Babler, B. L., Meade, M. R., et al. 2009, PASP, 121, 213

Dame, T. M., Hartmann, D., & Thaddeus, P. 2001, ApJ, 547, 792

Dame, T. M., & Thaddeus, P. 2011, ApJ, 734, L24

Hachisuka, K., Brunthaler, A., Menten, K. M., et al. 2009, ApJ, 696, 1981

Haschick, A. D., & Ho, P. T. P. 1985, ApJ, 292, 200

Honma, M., Bushimata, T., Choi, Y. K., et al. 2007, PASJ, 59, 889

Honma, M., Hirota, T., Kan-Ya, Y., et al. 2011, PASJ, 63, 17

Honma, M., Nagayama, T., Ando, K., et al. 2012, PASJ, 64, 136

Hou, L. G., & Han, J. L. 2014, A&A, 569, AA125

Kalberla, P. M. W., Dedes, L., Kerp, J., & Haud, U. 2007, A&A, 469, 511

Kalberla, P. M. W., & Kerp, J. 2009, ARA&A, 47, 27

Kennicutt, R., Jr., & Hodge, P. 1982, ApJ, 253, 101

Levine, E. S., Blitz, L., & Heiles, C. 2006, ApJ, 643, 881

McClure-Griffiths, N. M., Dickey, J. M., Gaensler, B. M., & Green, A. J. 2004, ApJ, 607, L127

Menten, K. M. 1991, ApJ, 380, L75

Minniti, D., Saito, R. K., Alonso-García, J., Lucas, P. W., & Hempel, M. 2011, ApJ, 733, LL43

Molinari, S., Brand, J., Cesaroni, R., & Palla, F. 2000, A&A, 355, 617

Nakanishi, H. and Sofue, Y., 2006, PASJ, 58, 847

Pestalozzi, M. R., Minier, V., & Booth, R. S. 2005, A&A, 432, 737

Plume, R., Jaffe, D. T., Evans, N. J., II, Martin-Pintado, J., & Gomez-Gonzalez, J. 1997, ApJ, 476, 730

Purcell, C. W., Bullock, J. S., Tollerud, E. J., Rocha, M., & Chakrabarti, S. 2011, Nature, 477, 301

Reid, M. J., Menten, K. M., Brunthaler, A., et al. 2009, ApJ, 693, 397

Reid, M. J., Menten, K. M., Zheng, X. W., et al. 2009, ApJ, 700, 137

Reid, M. J., Menten, K. M., Brunthaler, A., et al. 2014, ApJ, 783, 130

Rygl, K. L. J., Brunthaler, A., Reid, M. J., et al. 2010, A&A, 511, A2

Sanna, A., Reid, M. J., Dame, T. M., et al. 2012, ApJ, 745, 82

Sato, M., Reid, M. J., Brunthaler, A., & Menten, K. M. 2010, ApJ, 720, 1055

Schönrich, R., Binney, J., & Dehnen, W. 2010, MNRAS, 403, 1829

Szymczak, M., & Kus, A. J. 2000, A&A, 360, 311

Urquhart, J. S., Figura, C. C., Moore, T. J. T., et al. 2014, MNRAS, 437, 1791

Vallée, J. P. 2005, AJ, 130, 569

Wouterloot, J. G. A., Brand, J., & Henkel, C. 1988, A&A, 191, 323

Wouterloot, J. G. A., Brand, J., & Fiegle, K. 1993, A&AS, 98, 589

Wouterloot, J. G. A., Fiegle, K., Brand, J., & Winnewisser, G. 1995, A&A, 301, 236

Xu, Y., Li, J. J., Hachisuka, K., et al. 2008, A&A, 485, 729

Xu, Y., Li, J. J.,Reid, M. J., et al. 2013, ApJ, 769, 15

## 6. Online Material

This preprint was prepared with the AAS LaTeX macros v5.2.

Table 5: Results of Parallax and proper motion measurements.

| Maser | Background source | $v_{\rm LSR}$ (km s$^{-1}$) | Parallax (mas) | $\mu_\alpha$ (mas yr$^{-1}$) | $\mu_\delta$ (mas yr$^{-1}$) |
|---|---|---|---|---|---|
| G097.53+3.18 | J2127+5528 | –69.42 | 0.126 ± 0.027 | –2.69 ± 0.13 | –2.88 ± 0.07 |
| | J2139+5540 | –69.42 | 0.171 ± 0.023 | –2.71 ± 0.13 | –2.80 ± 0.06 |
| | J2123+5500 | –69.42 | 0.141 ± 0.018 | –2.66 ± 0.05 | –3.00 ± 0.13 |
| | J2117+5431 | –69.42 | 0.118 ± 0.016 | –2.62 ± 0.04 | –3.03 ± 0.12 |
| | Combined fit | –69.42 | 0.120 ± 0.014 | –2.67 ± 0.10 | –2.93 ± 0.10 |
| G097.53+3.18 | J2127+5528 | –69.84 | 0.066 ± 0.028 | –3.00 ± 0.09 | –2.74 ± 0.08 |
| | J2139+5540 | –69.84 | 0.117 ± 0.030 | –3.06 ± 0.11 | –2.79 ± 0.07 |
| | J2123+5500 | –69.84 | 0.074 ± 0.029 | –2.93 ± 0.08 | –2.80 ± 0.09 |
| | J2117+5431 | –69.84 | 0.065 ± 0.029 | –2.87 ± 0.08 | –2.78 ± 0.14 |
| | Combined fit | –69.84 | 0.070 ± 0.014 | –2.96 ± 0.09 | –2.78 ± 0.10 |
| G097.53+3.18 | J2127+5528 | –71.52 | 0.213 ± 0.015 | –3.60 ± 0.05 | –2.34 ± 0.22 |
| | J2139+5540 | –71.52 | 0.201 ± 0.029 | –3.57 ± 0.10 | –2.35 ± 0.11 |
| | J2123+5500 | –71.52 | 0.153 ± 0.023 | –3.19 ± 0.07 | –2.32 ± 0.26 |
| | J2117+5431 | –71.52 | 0.122 ± 0.038 | –3.09 ± 0.12 | –2.13 ± 0.29 |
| | Combined fit | –71.52 | 0.169 ± 0.017 | –3.36 ± 0.09 | –2.29 ± 0.23 |
| G097.53+3.18 | J2127+5528 | –71.94 | 0.221 ± 0.014 | –3.63 ± 0.04 | –2.38 ± 0.22 |
| | J2139+5540 | –71.94 | 0.214 ± 0.030 | –3.61 ± 0.09 | –2.40 ± 0.13 |
| | J2123+5500 | –71.94 | 0.162 ± 0.018 | –3.23 ± 0.06 | –2.36 ± 0.26 |
| | J2117+5431 | –71.94 | 0.132 ± 0.034 | –3.13 ± 0.10 | –2.18 ± 0.30 |
| | Combined fit | –71.94 | 0.177 ± 0.016 | –3.40 ± 0.08 | –2.33 ± 0.24 |
| G097.53+3.18 | J2127+5528 | –72.37 | 0.211 ± 0.010 | –3.63 ± 0.03 | –2.38 ± 0.22 |
| | J2139+5540 | –72.37 | 0.206 ± 0.025 | –3.61 ± 0.08 | –2.41 ± 0.13 |
| | J2123+5500 | –72.37 | 0.150 ± 0.021 | –3.21 ± 0.06 | –2.36 ± 0.26 |
| | J2117+5431 | –72.37 | 0.116 ± 0.040 | –3.11 ± 0.12 | –2.17 ± 0.30 |
| | Combined fit | –72.37 | 0.166 ± 0.016 | –3.39 ± 0.08 | –2.33 ± 0.24 |
| G097.53+3.18 | J2127+5528 | –77.00 | 0.117 ± 0.018 | –3.02 ± 0.05 | –2.34 ± 0.06 |
| | J2139+5540 | –77.00 | 0.145 ± 0.016 | –3.09 ± 0.05 | –2.37 ± 0.05 |
| | J2123+5500 | –77.00 | 0.164 ± 0.013 | –2.95 ± 0.03 | –2.42 ± 0.14 |
| | J2117+5431 | –77.00 | 0.147 ± 0.018 | –2.89 ± 0.04 | –2.40 ± 0.16 |
| | Combined fit | –77.00 | 0.140 ± 0.009 | –2.99 ± 0.04 | –2.42 ± 0.11 |
| G097.53+3.18 | J2127+5528 | –77.42 | 0.120 ± 0.019 | –3.03 ± 0.05 | –2.38 ± 0.07 |
| | J2139+5540 | –77.42 | 0.147 ± 0.016 | –3.09 ± 0.05 | –2.41 ± 0.05 |
| | J2123+5500 | –77.42 | 0.167 ± 0.013 | –2.95 ± 0.03 | –2.46 ± 0.14 |
| | J2117+5431 | –77.42 | 0.150 ± 0.018 | –2.89 ± 0.04 | –2.44 ± 0.16 |
| | Combined fit | –77.42 | 0.143 ± 0.009 | –2.99 ± 0.04 | –2.42 ± 0.11 |
| G097.53+3.18 | J2127+5528 | –77.84 | 0.209 ± 0.017 | –2.97 ± 0.04 | –2.32 ± 0.08 |
| | J2139+5540 | –77.84 | 0.237 ± 0.016 | –3.03 ± 0.05 | –2.36 ± 0.05 |
| | J2123+5500 | –77.84 | 0.242 ± 0.029 | –2.89 ± 0.07 | –2.40 ± 0.15 |
| | J2117+5431 | –77.84 | 0.230 ± 0.030 | –2.83 ± 0.08 | –2.38 ± 0.17 |
| | Combined fit | –77.84 | 0.228 ± 0.012 | –2.93 ± 0.06 | –2.37 ± 0.12 |
| G097.53+3.18 | J2127+5528 | –78.26 | 0.122 ± 0.018 | –2.37 ± 0.05 | –2.41 ± 0.10 |
| | J2139+5540 | –78.26 | 0.149 ± 0.016 | –2.43 ± 0.04 | –2.44 ± 0.06 |
| | J2123+5500 | –78.26 | 0.165 ± 0.016 | –2.29 ± 0.04 | –2.49 ± 0.16 |
| | J2117+5431 | –78.26 | 0.148 ± 0.022 | –2.23 ± 0.06 | –2.47 ± 0.19 |
| | Combined fit | –78.26 | 0.144 ± 0.010 | –2.33 ± 0.05 | –2.45 ± 0.14 |
| G097.53+3.18 | J2127+5528 | –78.69 | 0.090 ± 0.020 | –2.96 ± 0.05 | –2.23 ± 0.10 |
| | J2139+5540 | –78.69 | 0.124 ± 0.019 | –3.03 ± 0.05 | –2.26 ± 0.06 |
| | J2123+5500 | –78.69 | 0.129 ± 0.011 | –2.89 ± 0.03 | –2.31 ± 0.13 |
| | J2117+5431 | –78.69 | 0.112 ± 0.016 | –2.83 ± 0.04 | –2.28 ± 0.17 |
| | Combined fit | –78.69 | 0.109 ± 0.009 | –2.93 ± 0.04 | –2.27 ± 0.12 |
| G097.53+3.18 | J2127+5528 | –79.53 | 0.106 ± 0.017 | –2.46 ± 0.04 | –2.66 ± 0.07 |
| | J2139+5540 | –79.53 | 0.133 ± 0.016 | –2.53 ± 0.04 | –2.69 ± 0.06 |
| | J2123+5500 | –79.53 | 0.146 ± 0.015 | –2.39 ± 0.04 | –2.74 ± 0.13 |
| | J2117+5431 | –79.53 | 0.130 ± 0.020 | –2.33 ± 0.05 | –2.72 ± 0.15 |
| | Combined fit | –79.53 | 0.126 ± 0.009 | –2.43 ± 0.04 | –2.70 ± 0.11 |
| | Combined fit | | 0.133 ± 0.017 | | |
| | $<\mu>$ | –74.89 | | –2.94 ± 0.07 | –2.48 ± 0.16 |

Table 6: Results of Parallax and proper motion measurements.

| Maser | Background source | $v_{\rm LSR}$ (km s$^{-1}$) | Parallax (mas) | $\mu_\alpha$ (mas yr$^{-1}$) | $\mu_\delta$ (mas yr$^{-1}$) |
|---|---|---|---|---|---|
| G168.06+00.82 | J0512+4041 | –26.21 | 0.210 ± 0.019 | 0.77 ± 0.05 | –0.07 ± 0.04 |
| | J0523+3926 | –26.21 | 0.249 ± 0.028 | 0.74 ± 0.08 | 0.04 ± 0.06 |
| | J0509+3951 | –26.21 | 0.239 ± 0.028 | 0.85 ± 0.08 | –0.05 ± 0.11 |
| | Combined fit | –26.21 | 0.230 ± 0.024 | 0.79 ± 0.07 | –0.03 ± 0.08 |
| G168.06+00.82 | J0512+4041 | –28.74 | 0.177 ± 0.015 | 0.47 ± 0.04 | –1.10 ± 0.05 |
| | J0523+3926 | –28.74 | 0.210 ± 0.016 | 0.43 ± 0.05 | –0.99 ± 0.03 |
| | J0509+3951 | –28.74 | 0.204 ± 0.017 | 0.55 ± 0.05 | –1.08 ± 0.08 |
| | Combined fit | –28.74 | 0.194 ± 0.016 | 0. 48± 0.05 | –1.06 ± 0.06 |
| G168.06+00.82 | J0512+4041 | –29.16 | 0.193 ± 0.026 | 0.58 ± 0.07 | –1.00 ± 0.08 |
| | J0523+3926 | –29.16 | 0.222 ± 0.032 | 0.54 ± 0.09 | –0.89 ± 0.09 |
| | J0509+3951 | –29.16 | 0.219 ± 0.032 | 0.66 ± 0.09 | –0.98 ± 0.16 |
| | Combined fit | –29.16 | 0.211 ± 0.029 | 0. 59± 0.08 | –0.96± 0.12 |
| G168.06+00.82 | J0512+4041 | –29.58 | 0.156 ± 0.013 | 0.46 ± 0.04 | –1.14 ± 0.07 |
| | J0523+3926 | –29.58 | 0.182 ± 0.019 | 0.42 ± 0.05 | -1.02 ± 0.03 |
| | J0509+3951 | –29.58 | 0.179 ± 0.022 | 0.53 ± 0.06 | –1.12 ± 0.07 |
| | Combined fit | – 29.58 | 0.170 ± 0.019 | 0.47 ± 0.05 | –1.09 ± 0.06 |
| | Combined fit | | 0.201 ± 0.024 | | |
| | $<\mu>$ | –28.42 | | 0.58 ± 0.07 | –0.78 ± 0.08 |

Table 7: Results of Parallax and proper motion measurements.

| Maser | Background source | $v_{\rm LSR}$ (km s$^{-1}$) | Parallax (mas) | $\mu_\alpha$ (mas yr$^{-1}$) | $\mu_\delta$ (mas yr$^{-1}$) |
|---|---|---|---|---|---|
| G182.68–03.26 | J0540+2507 | –5.37 | 0.158 ± 0.045 | 0.74 ± 0.12 | –0.44 ± 0.14 |
| | J0540+2507 | –5.79 | 0.149 ± 0.042 | 0.74 ± 0.11 | –0.45 ± 0.13 |
| | J0540+2507 | –7.05 | 0.191 ± 0.042 | 0.01 ± 0.11 | –0.59 ± 0.14 |
| | J0540+2507 | –7.89 | 0.131 ± 0.044 | 0.26 ± 0.12 | –0.30 ± 0.12 |
| | Combined fit | | 0.157 ± 0.042 | | |
| | $<\mu>$ | –6.53 | | 0.44 ± 0.12 | –0.45 ± 0.13 |

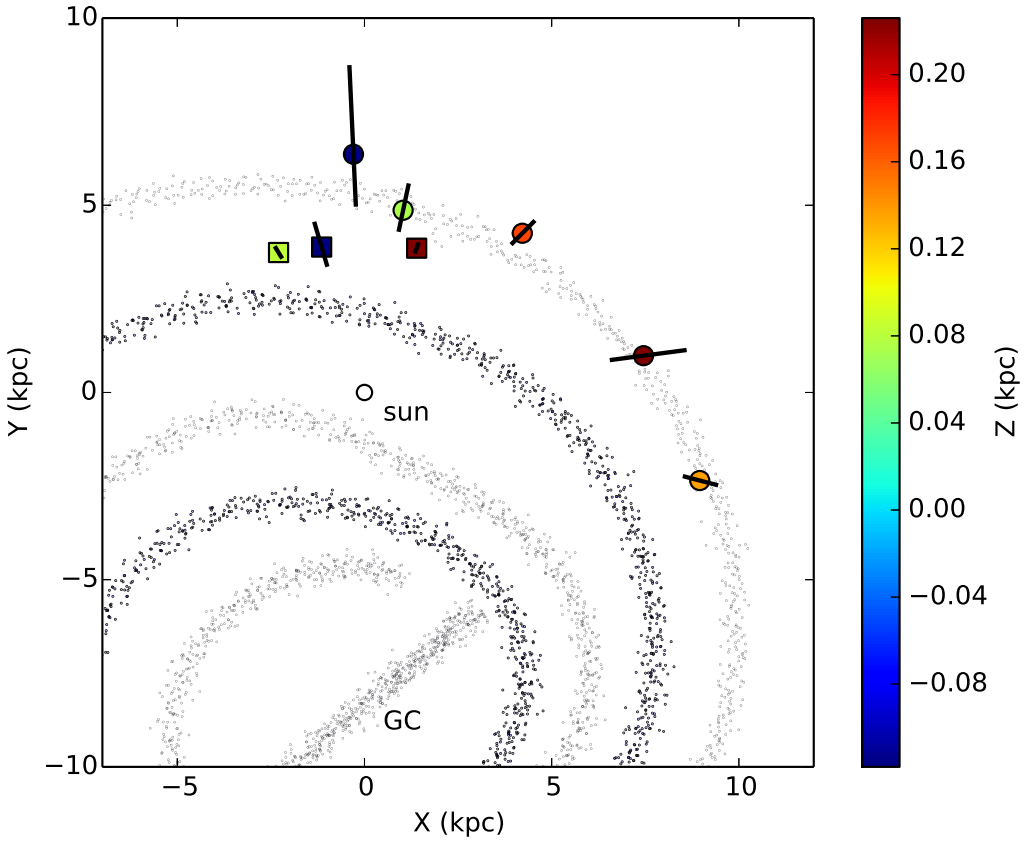


Fig. 7.— Location of 22 GHz water maser sources in the Outer Arm (filled circle) with error bar. Other 22 GHz water maser sources in the Outer Arm, G075.29+01.32 (Sanna et al. 2012) and G135.27+02.79 (Hachisuka et al. 2009), are also plotted (filled circle). Three 22 GHz water maser sources in the interarm (filled square), G160.14+03.15, G211.59+01.05 (Reid et al. 2014), and G196.45-01.67 (Asaki et al. 2014) are plotted. The color index shows the distance from the Galactic plane. The origin of figure is the location of Sun. The distance between Sun and Galactic center is 8.3 kpc.